
Self-supervised Representation Learning of Neuronal Morphologies

Marissa A. Weis^{1,2} Laura Pedo¹ Timo Lüddecke¹ Alexander S. Ecker^{1,3}

Abstract

Understanding the diversity of cell types and their function in the brain is one of the key challenges in neuroscience. The advent of large-scale datasets has given rise to the need of unbiased and quantitative approaches to cell type classification. We present GRAPHDINO, a purely data-driven approach to learning a low dimensional representation of the 3D morphology of neurons. GRAPHDINO is a novel graph representation learning method for spatial graphs utilizing self-supervised learning on transformer models. It smoothly interpolates between attention-based global interaction between nodes and classic graph convolutional processing. We show that this method is able to yield morphological cell type clustering that is comparable to manual feature-based classification and shows a good correspondence to expert-labeled cell types in two different species and cortical areas. Our method is applicable beyond neuroscience in settings where samples in a dataset are graphs and graph-level embeddings are desired.

1. Introduction

The brain is structured into different areas that contain diverse types of neurons (Ascoli et al., 2008). The morphology of cortical neurons is highly complex with widely varying shapes that are tightly linked to their function. For example, the axonal and dendritic processes of a neuron determine its connection to other cells and potentially areas (Goldberg et al., 2004; Oberlaender et al., 2012).

Cell morphology has long been used to classify neurons into cell types (Ramón y Cajal, 1911). Morphology-based classification has traditionally been carried out by either

laborious expert analysis through visual inspection (Ascoli et al., 2008; Defelipe et al., 2013) or by computing a set of predefined, quantitatively measurable features such as number of branching points (Uylings & Van Pelt, 2002; Scorcioni et al., 2008; Oberlaender et al., 2012; Polavaram et al., 2014; Markram et al., 2015; Lu et al., 2015).

Both approaches have deficits. The classification of neurons by experts has been shown to have a high variance, within and between expert annotators (Defelipe et al., 2013). Similarly, the definition of fixed morphological features for classification introduces biases into the classification process by only taking a limited set of features into account, for instance only certain neuronal compartments (Wang, 2018). These features might be specific to the studied neuronal population, complicating application to new areas or species, or one might overlook important features that are not immediately visible.

Recent advances in recording technologies have greatly accelerated data collection and therefore the amount of data available. Increasing dataset sizes render classifying all neurons manually infeasible, but provide optimal conditions to apply unsupervised machine learning methods. We propose to learn features from the 3D morphology of neurons in a purely data-driven fashion that allows the model to pick relevant features, thereby reducing the shortcomings introduced by explicit feature selection. We learn a low-dimensional representation of the 3D shape of each neuron that captures its essence. Using the learned feature space, we cluster neurons into morphological cell types.

Our contributions in this paper are threefold:

1. We propose a new self-supervised model to learn graph-level embeddings for spatial graphs.
2. We introduce a new attention module that takes the adjacency of graphs into account and can smoothly interpolate between transformer-style key-value attention and message passing between neighbors as in graph neural networks.
3. We apply this approach to the classification of excitatory neuronal morphologies and show that it produces clusters that are consistent with known excitatory cell types obtained by manual feature-based classification and expert-labeling.

¹Institute of Computer Science and Campus Institute Data Science, University of Göttingen, Germany ²Institute for Theoretical Physics, University of Tübingen, Germany ³Max Planck Institute for Dynamics and Self-Organization, Göttingen, Germany. Correspondence to: Marissa A. Weis <marissa.weis@uni-goettingen.de>.

2. Related Work

2.1. Cell type classification based on neuronal morphologies

Morphology has been used for a long time to classify neurons by either letting experts visually inspect the cells (Ramón y Cajal, 1911; Defelipe et al., 2013) or by specifying expert-defined features that can be extracted and used as input to a classifier (Oberlaender et al., 2012; Markram et al., 2015; Kanari et al., 2017; Wang, 2018; Kanari et al., 2019; Gouwens et al., 2019) (see Armañanzas & Ascoli (2015) for review). Ascoli et al. (2008) made an effort to unify the used expert-defined features.

With the advent of new technologies for microscopic imaging, electrical recording, and molecular analysis such as Patch-seq (Cadwell et al., 2015) and other methods that allowed the simultaneous recording of the transcriptome, electrophysiology and morphology of whole cells, several works have explored to predict cell types from multiple modalities (Gala et al., 2021) or to predict one modality from the other (Cadwell et al., 2015; Scala et al., 2021; Gouwens et al., 2020). Oberlaender et al. (2012) and Markram et al. (2015) classify neurons to build a model of a whole neural circuit.

Modeling neuronal morphologies. There are several works that try to learn a representation of neuronal morphologies. Laturnus & Berens (2021) propose a generative approach involving random walks in graphs to model neuronal morphologies. Schubert et al. (2019) process 2D projections of neuronal morphologies with a convolutional neural network (CNN) to learn low-dimensional representations. Seshamani et al. (2020) extract local mesh features around spines and combine them with traditional Sholl analysis (Sun et al., 1953). Gouwens et al. (2019) define a set of morphological features based on graphs and perform hierarchical clustering on them. We use the latter as a baseline for a classical approach with pre-defined features.

2.2. Graph Neural Networks (GNNs)

Graph neural networks learn node representations by recursively aggregating information from adjacent nodes as defined by the graph’s structure. While early approaches date back over a decade (Scarselli et al., 2008) recently numerous new variants were introduced for (semi-) supervised settings: relying on convolution over nodes (Duvinaud et al., 2015; Hamilton et al., 2017; Kipf & Welling, 2017), using recurrence (Li et al., 2016), or making use of attention mechanisms (Veličković et al., 2018). A representation for the whole graph is often derived by a readout operation on the node representations, for instance averaging. See Dwivedi et al. (2020) for a recent benchmark on graph neural network architectures.

Transformer-based GNNs. Zhang et al. (2020) and Dwivedi & Bresson (2021), similar to us, use transformer attention to work with graphs.

However, Zhang et al. (2020) compute transformer attention over the nodes of sampled subgraphs, while Dwivedi & Bresson (2021) compute the attention only over local neighbors of nodes, which boils down to a weighted message passing that is conditioned on node feature similarity, and trains supervised.

Unlike previous approaches, we compute the attention between nodes of the global graph and adapt the transformer attention to consider the adjacency matrix of the graph, which gives the model the flexibility to trade-off taking the neighbors of a node into account versus all other nodes in the graph.

Contrastive learning on graphs. Contrastive learning has proven to be a useful technique for training image feature extractors (Oord et al., 2018; Chen et al., 2020; Chen & He, 2021; Caron et al., 2021) and has been investigated for learning graph (Li et al., 2016; Hassani & Khasahmadi, 2020; Qiu et al., 2020; Xu et al., 2021) and node (Veličković et al., 2019) representations.

Narayanan et al. (2017) learn graph representations through skip-gram with negative sampling by predicting present subgraphs. Sun et al. (2020) learn graph-level representations in a contrastive way, by predicting if a node and a graph representation originate from the same graph. Similarly, Hassani & Khasahmadi (2020) put node features of one view in contrast with the graph encoding of a second view and vice versa. They build on graph diffusion networks (Klicpera et al., 2019) and only augment the structure of the graph but not the initial node features. Qiu et al. (2020) propose a generic pre-training method which uses an InfoNCE objective (Oord et al., 2018) to learn features by telling augmented versions of one subgraph from other subgraphs. For augmentation, random walks are used. Xu et al. (2021) aim to capture local and global structures for whole-graph representation learning. To this end, they rely on an EM-like algorithm to jointly train the assignment of graphs to hierarchical prototypes, the GNN parameters and the prototypes. Zhu et al. (2021) propose adaptive augmentation, which considers node centrality and importance to generate graph views in a contrastive framework.

Unlike prior work, we contrast two global views of a graph in order to learn a whole-graph representation. Our method operates on spatially embedded graphs, in which nodes correspond to points in 3D space. We make use of this knowledge in the choice of our augmentations.

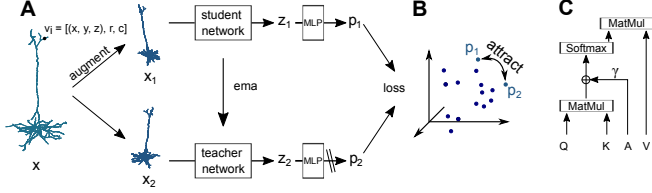


Figure 1. **A.** Model architecture. During training the graph of the neuronal skeleton x with node features $v_i \in V = \{v_i\}_{i=1}^N$ is transformed into two views x_1 and x_2 through graph augmentation and encoded by two neural networks that consist of multiple graph attention modules. The student network is trained using gradient descent, while the weights of the teacher network are an exponential moving average (ema) of the student weights. **B.** Latent vectors p_1 and p_2 are optimized to be close to each other. **C.** Graph attention is an adaptation of standard transformer attention (Vaswani et al., 2017) with a learned bias of the attention matrix towards the graph adjacency matrix A .

3. Methods

We propose GRAPHDINO, an adaptation of DINO (Caron et al., 2021), to work on graph data with the following alterations: (1) we incorporate the graph’s adjacency matrix into the attention computation; (2) we use the graph Laplacian as positional encoding; (3) we define augmentations suitable for spatial graphs. In this section, we first describe DINO and then our adaptations.

3.1. DINO

DINO is a self-supervised model for learning latent representations of images, that can then be used to perform image classification or other downstream tasks. DINO consists of a student network g_{θ_s} and a teacher network g_{θ_t} . Both have the same backbone architecture, namely a transformer. During training, the student and the teacher network receive two random transformations of an input image. The output of both networks $z \in \mathbb{R}^{B \times D}$ is normalized with a softmax with different temperatures over the feature dimension D . In the case of the teacher network, previous to applying the softmax, a centering with the mean over the batch is performed. Only the weights θ_s of the student network are optimized using gradient descent, while the weights of the teacher network θ_t are updated using an exponential moving average (ema) of the student weights. The latent vectors z_1 and z_2 are processed by a multi-layer perceptron (MLP) that outputs p_1 and p_2 , over which the cross-entropy loss is computed.

3.2. GRAPHDINO

GRAPHDINO is a self-supervised model for learning latent representations of graphs (Fig. 1). In order to use information given by the connectivity of the graph, we mod-

ify the computation of the transformer attention to take the graph adjacency matrix into account and use the graph Laplacian as positional encoding. Furthermore, we simplify the DINO architecture by removing the l_2 normalization and the weight normalized fully-connected layer from the projection head and we do not differentiate between the augmentations seen by the student and the teacher network.

Input. Input to the network is the 3D shape of a neuron which is represented as an undirected graph $G = (V, E)$. V is the set of nodes $\{v_i\}_{i=1}^N$ and E the set of undirected edges $E = \{e_{ij} = (v_i, v_j)\}$ that connect two nodes v_i, v_j . The features of each node v_i in the graph are encoded into a token using a linear transformation. These tokens are then used as input to the transformer model, which consists of seven multi-head attention modules with eight heads.

Attention bias. Key-value query attention became popular in natural language modelling (Vaswani et al., 2017). It is computed as follows:

$$Attention(Q, K, V) = \sigma\left(\frac{QK^T}{\sqrt{d_k}}\right) V,$$

where K are the keys, Q are the queries and V are the values. Keys, queries and values are each computed as a learned linear projection of the input tokens. $\sigma(\cdot)$ denotes the softmax activation function.

To make use of the information given by the adjacency matrix A of the input graph — i.e. the neighborhood of nodes —, we bias the attention towards A by adding a learned bias to the attention matrix M that is conditioned on the input token values:

$$\lambda_i, \gamma_i = Wx_i,$$

$$Attention(Q, K, V) = \sigma\left(\lambda \frac{QK^T}{\sqrt{d_k}} + \gamma A\right) V,$$

where $x_i \in \mathbb{R}^D$ is the token of node i , $W \in \mathbb{R}^{2 \times D}$ is a learned weight matrix, $\lambda, \gamma \in \mathbb{R}^N$ are two learned factors per node that trade off how much weight is assigned to neighboring nodes versus all other nodes in the graph, $A \in \mathbb{R}^{N \times N}$ is the adjacency matrix of the input graph, and N is the number of nodes in the graph.

In the most extreme case, the attention matrix is dominated by A and the transformer attention computation gets similar to the message passing algorithm that is commonly used when working with graphs (Scarselli et al., 2009; Duvenaud et al., 2015; Gilmer et al., 2017). But GRAPHDINO is more flexible than regular message passing since it can decide how much weight is given to the neighbors of a node while maintaining the flexibility to attend to all other nodes in the graph as well.

Positional Encoding. Following Dwivedi et al. (2020), we use the normalized graph Laplacian matrix as positional encoding, which is computed as follows:

$$L = I - D^{-1/2}AD^{-1/2} = U^T\Lambda U,$$

where D is the $N \times N$ degree matrix and A is the $N \times N$ adjacency matrix of the graph with N nodes, and U and Λ are the matrices of eigenvectors and eigenvalues, respectively. As positional encodings we take the first k eigenvectors with largest eigenvalues. In our experiments we set $k = 32$.

Data augmentation. Data augmentation plays an important role in self-supervised learning and needs to be adapted to the data, since it expresses which invariances should be imposed. Given the spatial neuronal data, we apply the following augmentations: (1) subsampling: we subsample the original graph to a fixed number 200 nodes in order to facilitate batch processing. Furthermore, this augmentation retains the global structure of the neuron, while altering local structure in the two views. (2) rotation: we perform random 3D rotation around the y-axis, that is orthogonal to the pia. (3) jittering: we randomly translate the node position by adding Gaussian noise with $\mathcal{N}(0, \sigma)$ (4) subgraph deletion: we delete n random branches of the graph while maintaining its overall structure. (5) cumulative jittering: we cumulatively alter the node position along n branches by cumulatively adding Gaussian noise with $\mathcal{N}(0, \sigma)$. (6) soma depth: we randomly translate the soma depth by adding Gaussian noise with $\mathcal{N}(0, \sigma)$ along the y-axis.

4. Experiments

4.1. Data

Allen Brain Atlas: Mouse visual cortex. We use the Allen Brain Atlas dataset that contains 568 neurons from the mouse visual cortex with a broad coverage of types, layers and transgenic lines. The dataset is accessible as part of the Allen Cell Types Database.¹ We will refer to this dataset as the Allen Brain Atlas (ABA) dataset.

See Allen Institute (2016) for details on how the dataset was recorded. The dataset contains a classification of each neuron into spiny and aspiny or sparsely spiny cells, which are assumed to be excitatory and inhibitory neurons, respectively (Gouwens et al., 2019). Additionally, the dataset provides information on the cortical layer the neuron was recorded from. To be comparable to previous work, we only use the 430 neurons also used by Gouwens et al. (2019). They consist of 230 spiny and 200 aspiny neurons. Following Gouwens et al. (2019), we summarize the sparsely spiny

¹<http://celltypes.brain-map.org/>

and aspiny cells into one class, which we will subsequently refer to as aspiny neurons.

Blue Brain Project: Rat somatosensory cortex. As a second dataset, we use a large dataset of juvenile rat somatosensory cortex morphologies from the Neocortical Microcircuit Collaboration Portal of the Blue Brain Project (Ramaswamy et al., 2015). It contains 1009 neurons, from which 616 are labeled by experts into cell types and cortical layer. We will refer to this dataset as the Blue Brain Project (BBP) dataset. In contrast to the ABA dataset, it does not contain information on relative soma depth with respect to the pia for individual neurons. Therefore, we normalize node positions with respect to the corresponding soma location (which is set to $(0, 0, 0)$). Additionally, we remove axons from the graphs, since their quality of reconstruction in the dataset is noisy due to using slicing as a recording method.

Preprocessing. In order to speed up training, we subsample the graph of each neuron to 1000 nodes and ensure that it contains only one connected component. If there are unconnected components, we connected them by adding an edge between two nodes of two unconnected components that have the least distance between their spatial coordinates. Neurons are aligned to the pia.

Node features. The nodes V are defined by their node features $v_i = [s, r, c]$ with $s \in \mathbb{R}^3$ representing the spatial xyz-coordinates, r the radius of the volume at node v_i and c a one-hot encoding of the compartments (soma, axon, basal dendrite, apical dendrite) (Fig. 1). Spatial coordinates are normalized such that the soma spatial position is either $(0, 0, d)$, where d is the soma depth for the ABA dataset or $(0, 0, 0)$ for the BBP dataset.

4.2. Training details

GRAPHDINO is implemented in PyTorch (Paszke et al., 2019) and trained with the Adam optimizer (Kingma & Ba, 2015) with a batch size of 64 for 100,000 iterations for the ABA dataset and 200,000 iterations for the BBP dataset. The learning rate is linearly increased to $1e^{-4}$ during the first 2,000 iterations and then decayed using a cosine schedule (Loshchilov & Hutter, 2016). The dimensionality of the latent representation z is set to 32 and the dimensionality of the projection p is 1,000.

We split the dataset in 90% training data and 10% validation data. To verify that our model does not overfit, we visualize the distribution of the latent embeddings of training and validation set (see Appendix A Fig. A.1). All analyses regarding cell types will subsequently be performed on the whole dataset to ensure sufficient coverage of all cell types and layers.

| Model | Accuracy | Model | Accuracy |
|--------------------|----------------|----------------|----------------|
| Ours | 51.5 \pm 1.3 | Ours | 51.5 \pm 1.3 |
| – attention bias | 54.2 | – 3D rot. | 32.6 |
| – positional enc. | 50.6 | – cum. jit. | 56.8 |
| – soma depth | 53.3 | – node jitter | 54.0 |
| – neural comp. | 54.3 | – soma jitter | 48.9 |
| teacher temp. 0.04 | 48.4 | – drop branch | 52.0 |
| | | 100 nodes | 51.8 |
| Minimal | 29.7 | Minimal | 29.7 |
| + attention bias | 31.2 | + cum. jit. | 28.3 |
| + positional enc. | 37.5 | + node jitter | 33.8 |
| + soma depth | 47.8 | + soma jitter | 30.2 |
| + neural comp. | 33.2 | + drop branch | 33.8 |
| | | 200 nodes | 31.5 |

(a) Architectural and input feature choices.

(b) Different data augmentation choices.

Table 1. Ablation study results. Performance of our full model averaged over five random seeds and given as mean \pm standard deviation. “–” means removing one component from the full model; “+” means adding one component to the minimal model.

We use scipy for clustering (Pedregosa et al., 2011).

4.3. Ablations

To test which architecture choices and augmentations have a strong effect on the performance of our model, we conduct two ablation studies on the ABA dataset. First, we remove one component from our model at a time and evaluate performance to identify necessary components. Second, we define a minimal model by removing all non-necessary components and add one component at a time, to test whether any of the augmentations are sufficient.

To assess the quality of the learned representation, we train the models self-supervised on the ABA dataset. We then treat the Gouwens et al. (2019) clusters as if they were ground truth labels and train a random forest classifier to predict those class labels from our learned representations. For further details, see Appendix B.

Removing individual components from the model does not impact the performance significantly, neither in terms of architectural features (Tab. 1a) nor for data augmentations (Tab. 1b) — except for 3D rotation. Conversely, none of the components on its own is sufficient: We defined a minimal model that keeps only 3D rotation but drops all other augmentations and architectural features. This minimal model performs significantly worse than our standard model (29.7 % vs. 51.5 % accuracy; Tab. 1). The only component that by itself leads to a substantial boost over the minimal model is information about the soma depth (expected, since it almost perfectly codes the layer), but it is still not sufficient to reach full performance. Taken together, individual components can be compensated for by others, but it is necessary to use a diverse set of them to reach full performance.

Since the ablations results suggest that we might augment somewhat too aggressively on the ABA dataset, we decrease the strength of the augmentations when training on the BBP dataset and remove the cumulative jittering.

For all subsequent results, augmentation parameters for ABA are: $\sigma = 1$ for jittering (3), $n = 10$ for subgraph deletion, $n = 5$ for cumulative jittering with $\sigma = 0.5$ and $\sigma = 10$ for soma translation. For BBP, we subsample the graph to 100 nodes and set $\sigma = 0.1$ for jittering (3), $n = 5$ for subgraph deletion, $n = 0$ for cumulative jittering and $\sigma = 1$ for soma translation.

5. Results

In the following, we analyze the low-dimensional representation of the neuronal morphologies obtained by training the model on the ABA dataset as well as the BBP dataset. We first visualize the representations using t-distributed stochastic neighbor embedding (t-SNE) (van der Maaten & Hinton, 2008). Subsequently, we qualitatively show that cells of the same types form clusters in our learned representation. We verify our clustering analysis by showing that we can predict cluster labels of held-out portions of the data. Finally, we compare our results for the ABA dataset to the clustering obtained on the same neurons using the approach of Gouwens et al. (2019) and for the BBP dataset to expert labels given by Markram et al. (2015).

5.1. Morphological embeddings differentiate between spiny/aspiny cells and layers

We first use t-SNE to map the learned embeddings of the ABA dataset into 2D and visualize them (Fig. 2). A clear separation between spiny and aspiny neurons can be observed (see Fig. 2A), indicating that our learned representation captures meaningful biological differences of the neuronal morphologies.

Next, we ask whether the learned embeddings capture the laminar location of the neurons. Indeed, this is the case (Fig. 2B): For the aspiny neurons (lower cluster), adjacent layers are also adjacent in the embedding, i.e. layer 1 (L1) neurons are next to layer 2/3 (L2/3) neurons etc.; the same is true for the spiny neurons (upper cluster).

Interestingly, some of the spiny L2/3 neurons end up in the aspiny cluster in the layer 2/3 region. These are the wide and short L2/3 neurons, whose size and dendritic tree is morphologically similar to aspiny neurons in the same layer. Furthermore, they are one of the few spiny cells with an extensively recorded axonal tree, similar to the aspiny neurons.

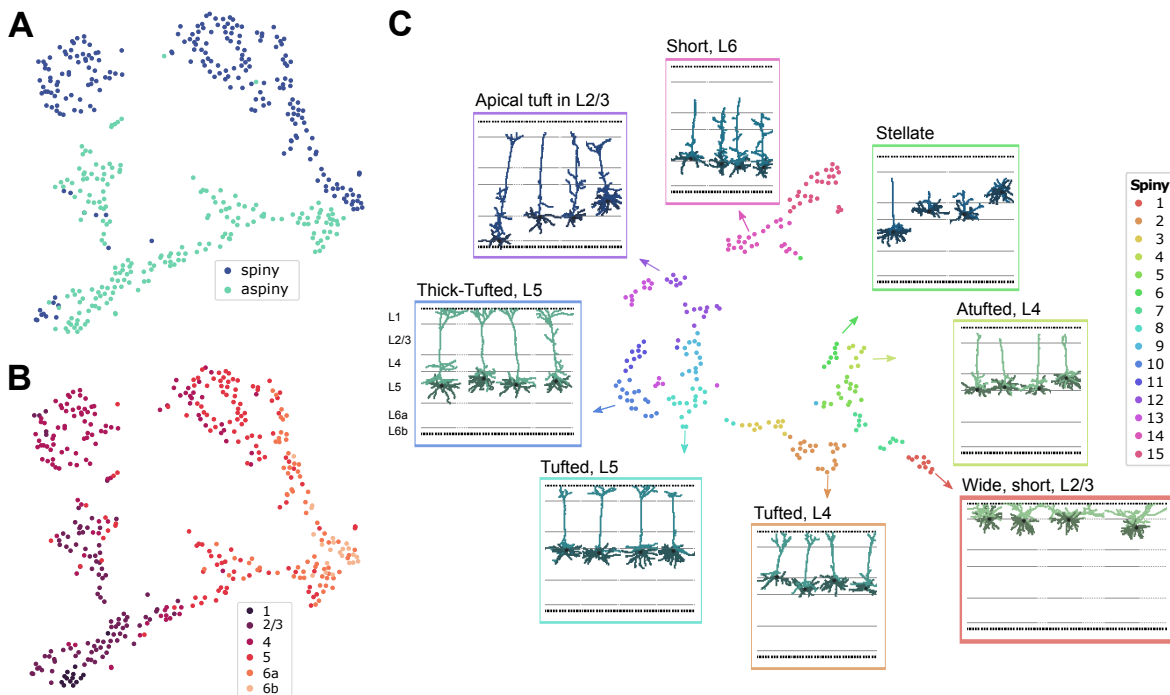


Figure 2. t-SNE embedding (perplexity=30) of latent representation of 3D neuron morphologies of the ABA dataset showing (A) a separation into spiny and aspiny neurons and (B) a separation into neurons with different cortical layers of origin. C. t-SNE embedding (perplexity=10) of the latent representations of the morphologies of the spiny neurons colored by the cluster found by our model. Example neurons for some of the clusters are shown in the corresponding boxes. Apical dendrites are shown in lighter color, while basal dendrites are colored darker. Soma is indicated by black circle. Lines show averaged cortical layer boundaries.

5.2. Morphological embeddings recover known excitatory cell types

To identify cell types, we fit a Gaussian mixture model (GMM) with a diagonal covariance matrix to our learned representation of the spiny neurons. To determine the number of clusters, we fit 100 GMMs with different random seeds using five-fold cross-validation for 2–30 clusters. We average over the log-likelihood for each number of clusters over repetitions and folds. For the ABA dataset, we find $n = 15$ to be the best number of clusters and for the BBP dataset $n = 12$ (Fig. 3). We will use these numbers of clusters for all subsequent evaluations.

Having identified the optimal number of clusters, we re-fit the GMM to the full dataset including all neurons. To avoid picking a particularly good or bad random clustering, we fit 100 models and choose the one that has the highest average adjusted rand index (ARI) to all other clusterings.

The spiny neurons cluster nicely into different shapes and layers (Fig. 2C and Appendix Fig. B.3). For instance, cluster 10 groups thick-tufted pyramidal cells from layer 5, while cluster 1 contains wide and short neurons from layer 2/3 and cluster 4 contains atufted cells from layer 4.

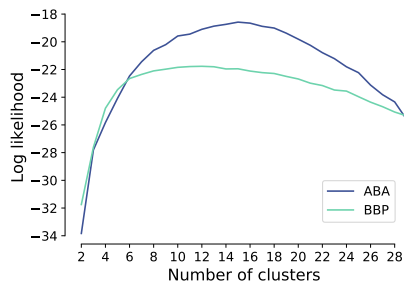


Figure 3. Log-likelihood of Gaussian Mixture Model on held-out test set for spiny neurons of Allen Brain Atlas (blue curve) and Blue Brain Project (turquoise curve) datasets.

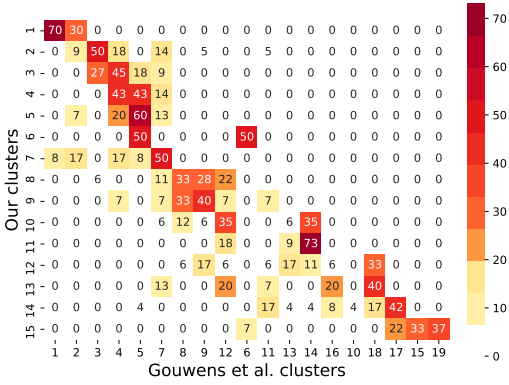


Figure 4. Confusion matrix between our and Gouwens et al. (2019) cluster assignments, in percentage, normalized along rows. Note that due to rounding errors not all rows sum to 100.

Cluster 6 contains stellate cells with some additional atufted cells (Fig. 2C, light green). These misplaced cells could be caused by our aggressive data augmentation, which stochastically removes branches during training, which might occasionally delete the atufted apical branch.

Most clusters show a strong preference for grouping cells whose soma position is in a certain layer. One interesting exception is cluster 12 (Fig. 2C, purple), which groups cells together whose apical tuft ends already in layer 2/3 — in contrast to most other pyramidal cells whose tuft extends fully into layer 1.

5.3. Data-driven clusters are consistent with previous studies

Gouwens et al. (2019) extracted expert-defined features from the graphs of the neurons from the ABA dataset and performed hierarchical clustering followed by additional automatic and manual post-processing steps to identify cell types. They identified 19 spiny cell type clusters. Our method produces clusters which are broadly consistent with their clustering (Fig. 4), but in a fully automated way and without pre-defining features.

For example, Gouwens et al. (2019) found two clusters that contain wide, short L2/3 cells (clusters 1 and 2), which are clustered in one cluster in our clustering, namely cluster 1, while their cluster 2 also contains some neurons from layer 4 (Fig. B.3).

Similarly, our clusters 2–5 contain pyramidal neurons from layer 4, being grouped by the amount of tuft on the apical dendrite (cluster 2: tufted, cluster 3: sparsely tufted, cluster 4: atufted with apical dendrite ending in L1, cluster 5: atufted with apical dendrite ending in L2/3). These correspond to clusters 3, 4, 5 and 7 of the Gouwens clustering, which also contain primarily layer 4 pyramidal cells mixed

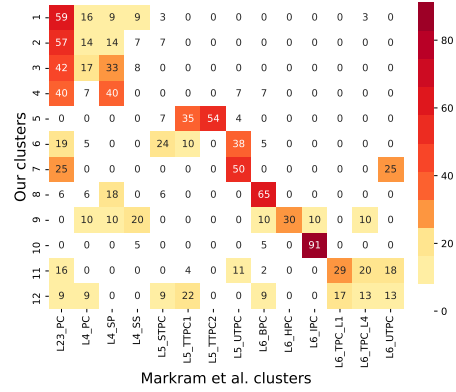


Figure 5. Confusion matrix between our clustering and expert labels on the BBP dataset, in percentage, normalized along rows. Note that due to rounding errors not all rows sum to 100.

with some deeper layer cells, that show different amounts of tuftedness. See also Fig. A.2 in Appendix A for the layer distribution over the clusters.

Both clusterings look comparable, with some notable differences such as Gouwens et al. (2019) find a cluster of narrow L6 cells (cluster 18, Fig. B.3) that is missing in our clustering. Conversely, our clustering, especially for the L2–5 cells, seems to cluster better by cortical layer. In addition, it identified the cells with apical dendrites ending in layer 2/3 (cluster 12, Fig. B.3), a feature that has not been picked up by clustering earlier manually defined features.

Gouwens et al. (2019) tested the predictability of their clusters by training a random forest classifier on out-of-bag prediction accuracy. They achieved an accuracy of 79% using their features. The same analysis on our labels and our features yields a substantially higher accuracy of 97%.

5.4. Data-driven clusters are consistent with expert labels

So far we have compared our clustering to an earlier unsupervised clustering approach. This comparison is difficult to quantify, since there is no objective ground truth information available. We therefore trained on a second dataset, the BBP dataset, which comes with cell type labels that have been manually assigned by experts in the field (Markram et al., 2015).

We first use t-SNE to map the learned embeddings into 2D and visualize them (Fig. 6). A good separation between spiny and aspiny neurons can be observed (Fig. 6a). We also observe some clustering into laminar layers, i.e. layer 5 (L5) spiny neurons in the left cluster and L1 aspiny neurons (right), but it is less pronounced than for the ABA dataset. This is most likely due to the fact that, in contrast to the ABA dataset, BBP does not come with a relative soma depth

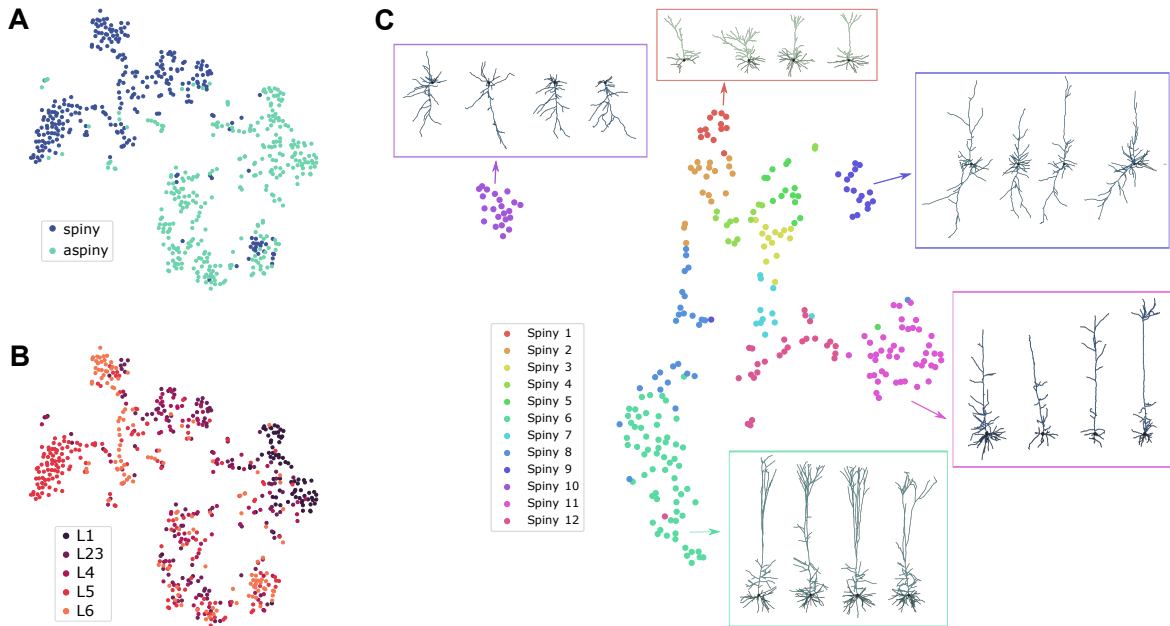


Figure 6. t-SNE embedding of latent representation of 3D neuronal morphologies of 616 labeled neurons from the BBP dataset colored by (A) spiny and aspiny neurons and (B) cortical layers of origin. (C) t-SNE embedding of 286 spiny neurons of BBP dataset colored by our clusters found via GMM. Example neurons for some of the clusters are shown in the corresponding boxes. Apical dendrites are shown in lighter color, while basal dendrites are colored darker. Soma is indicated by black circle.

for individual cells, making it difficult to separate neurons with similar morphologies that come from different layers.

We identified 12 clusters using GMM for the spiny neurons of the BBP dataset (Fig. 6). We test the predictability of our learned clusters by training a random forest classifier in out-of-bag prediction setting achieving an accuracy of 92.9%. Computing the adjusted rand index (ARI) between our clusters and the expert-identified neurons gave a performance of 0.29, which is higher than previous automated clustering methods. We achieve this performance on the same data while using significantly less prior information. In comparison, Gouwens et al. (2019) reached an ARI of 0.27 with a feature space specifically designed for spiny neurons and by splitting the neurons into their cortical layer of origin before performing the clustering. Their approach therefore reduces the complexity of the problem significantly, since misassignments across layers are excluded by construction.

Our method is reasonably consistent with the expert labels (Fig. 5). Similar to previous work (Gouwens et al., 2019; Kanari et al., 2019), our clustering splits the layer 2/3 neurons into multiple subtypes (our clusters 1–5), but merges the two groups of L5 tufted pyramidal cells (our cluster 6). L6 inverted pyramidal are almost perfectly recovered (our cluster 10), while our cluster 12 collects “outlier” cells that do not fit well in any of the remaining clusters — a behavior typical for GMMs — and does not correspond to a specific biological cell type.

5.5. Limitations

Our methods uses the skeleton of the 3D shape of a neuron in order learn relevant features for cell type classification. We have not taken some features into account that have been previously used to differentiate cell types, such as the shape of the soma (as formerly used for GABAergic interneurons) or spine densities (Ascoli et al., 2008). Future work could focus on incorporating them into our framework. Depending on the type of feature, they could be either integrated by adding them as features of the graph or as additional node features.

6. Conclusion

Increasingly large and complex datasets of neurons have given rise to the need of unbiased and quantitative approaches to cell type classification. We have demonstrated one such approach that is purely data-driven and self-supervised, and that learns a low-dimensional representation of the 3D shape of a neuron. By using self-supervised learning, we do not pre-specify which cell types to learn and which features to use, thereby reducing bias in the classification process and opening up the possibility to discover new cell types. A similar approach could also be useful in other domains beyond neuroscience, where samples of the dataset are spatial graphs and graph-level embeddings are desired, such as tree classification in forestry.

Acknowledgements

We thank the International Max Planck Research School for Intelligent Systems (IMPRS-IS), Tübingen, for supporting Marissa A. Weis.

References

- Allen Institute. Allen cell types database technical white paper: Morphology. 2016. URL http://help.brain-map.org/download/attachments/8323525/CellTypes_Morph_Overview.pdf.
- Armañanzas, R. and Ascoli, G. A. Towards the automatic classification of neurons. *Trends in Neurosciences*, 38(5): 307–318, 2015.
- Ascoli, G., Alonso-Nanclares, L., Anderson, S., Barrionuevo, G., Benavides-Piccione, R., Burkhalter, A., Buzsáki, G., Cauli, B., Defelipe, J., and Fairen, A. Petilla terminology: nomenclature of features of GABAergic interneurons of the cerebral cortex. *Nature reviews. Neuroscience*, 9:557–568, 2008.
- Cadwell, C., Palasantza, A., Jiang, X., Berens, P., Deng, Q., Yilmaz, M., Reimer, J., Shen, S., Bethge, M., Tolias, K., Sandberg, R., and Tolias, A. Electrophysiological, transcriptomic and morphologic profiling of single neurons using patch-seq. *Nature Biotechnology*, 34, 2015.
- Caron, M., Touvron, H., Misra, I., Jégou, H., Mairal, J., Bojanowski, P., and Joulin, A. Emerging properties in self-supervised vision transformers. In *Proceedings of the IEEE/CVF International Conference on Computer Vision (ICCV)*, pp. 9650–9660, 2021.
- Chen, T., Kornblith, S., Norouzi, M., and Hinton, G. A simple framework for contrastive learning of visual representations. In *Proc. of the International Conf. on Machine learning (ICML)*, 2020.
- Chen, X. and He, K. Exploring simple siamese representation learning. In *Proc. IEEE Conf. on Computer Vision and Pattern Recognition (CVPR)*, 2021.
- Defelipe, J., López-Cruz, P., Benavides-Piccione, R., Bielza, C., Larranaga, P., Anderson, S., Burkhalter, A., Cauli, B., Fairen, A., Feldmeyer, D., Fishell, G., Fitzpatrick, D., Freund, T., Gonzalez Burgos, G., Hestrin, S., Hill, S., Hof, P., Huang, J., Jones, E., and Ascoli, G. New insights into the classification and nomenclature of cortical gabaergic interneurons. *Nature reviews. Neuroscience*, 14, 2013.
- Duvenaud, D. K., Maclaurin, D., Iparraguirre, J., Bombarell, R., Hirzel, T., Aspuru-Guzik, A., and Adams, R. P. Convolutional networks on graphs for learning molecular fingerprints. In *Advances in Neural Information Processing Systems (NeurIPS)*, volume 28, 2015.
- Dwivedi, V. P. and Bresson, X. A generalization of transformer networks to graphs. *arXiv.org*, 2012.09699, 2021.
- Dwivedi, V. P., Joshi, C. K., Laurent, T., Bengio, Y., and Bresson, X. Benchmarking graph neural networks. *arXiv.org*, 2003.00982, 2020.
- Gala, R., Budzillo, A., Baftizadeh, F., Miller, J., Gouwens, N., Arkhipov, A., Murphy, G., Tasic, B., Zeng, H., Hawrylycz, M., et al. Consistent cross-modal identification of cortical neurons with coupled autoencoders. *Nature Computational Science*, 1(2):120–127, 2021.
- Gilmer, J., Schoenholz, S. S., Riley, P. F., Vinyals, O., and Dahl, G. E. Neural message passing for quantum chemistry. In *Proc. of the International Conf. on Machine learning (ICML)*, pp. 1263–1272, 2017.
- Goldberg, J. H., Lacefield, C. O., and Yuste, R. Global dendritic calcium spikes in mouse layer 5 low threshold spiking interneurons: implications for control of pyramidal cell bursting. *The Journal of physiology*, 558(2): 465–478, 2004.
- Gouwens, N., Sorensen, S., Berg, J., Lee, C., Jarsky, T., Ting, J., Sunkin, S., Feng, D., Anastassiou, C., Barkan, E., Bickley, K., Blesie, N., Braun, T., Brouner, K., Budzillo, A., Caldejon, S., Casper, T., Castelli, D., Chong, P., and Koch, C. Classification of electrophysiological and morphological neuron types in the mouse visual cortex. *Nature Neuroscience*, 22, 2019.
- Gouwens, N. W., Sorensen, S. A., Baftizadeh, F., Budzillo, A., Lee, B. R., Jarsky, T., Alfiler, L., Baker, K., Barkan, E., Berry, K., Bertagnolli, D., Bickley, K., Bomben, J., Braun, T., Brouner, K., Casper, T., Crichton, K., Daigle, T. L., Dalley, R., de Frates, R. A., Dee, N., Desta, T., Lee, S. D., Dotson, N., Egdorf, T., Ellingwood, L., Enstrom, R., Esposito, L., Farrell, C., Feng, D., Fong, O., Gala, R., Gamlin, C., Gary, A., Glandon, A., Goldy, J., Gorham, M., Graybuck, L., Gu, H., Hadley, K., Hawrylycz, M. J., Henry, A. M., Hill, D., Hupp, M., Kebede, S., Kim, T. K., Kim, L., Kroll, M., Lee, C., Link, K. E., Mallory, M., Mann, R., Maxwell, M., McGraw, M., McMillen, D., Mukora, A., Ng, L., Ng, L., Ngo, K., Nicovich, P. R., Oldre, A., Park, D., Peng, H., Penn, O., Pham, T., Pom, A., Popović, Z., Potekhina, L., Rajanbabu, R., Ransford, S., Reid, D., Rimorin, C., Robertson, M., Ronellenfitch, K., Ruiz, A., Sandman, D., Smith, K., Sulc, J., Sunkin, S. M., Szafer, A., Tieu, M., Torkelson, A., Trinh, J., Tung, H., Wakeman, W., Ward, K., Williams, G., Zhou, Z., Ting, J. T., Arkhipov, A., Sümbül, U., Lein, E. S., Koch, C., Yao, Z., Tasic, B., Berg, J., Murphy, G. J., and Zeng, H. Integrated morphoelectric and transcriptomic classification of cortical gabaergic cells. *Cell*, 183(4): 935–953.e19, 2020.

- Hamilton, W. L., Ying, R., and Leskovec, J. Inductive representation learning on large graphs. In *Advances in Neural Information Processing Systems (NeurIPS)*, pp. 1025–1035, 2017.
- Hassani, K. and Khasahmadi, A. H. Contrastive multi-view representation learning on graphs. In *Proc. of the International Conf. on Machine learning (ICML)*, volume 119, pp. 4116–4126, 2020.
- Kanari, L., Dlotko, P., Scolamiero, M., Levi, R., Shillcock, J. C., Hess, K., and Markram, H. A topological representation of branching neuronal morphologies. *Neuroinformatics*, 16:3 – 13, 2017.
- Kanari, L., Ramaswamy, S., Shi, Y., Morand, S., Meystre, J., Perin, R., Abdellah, M., Wang, Y., Hess, K., and Markram, H. Objective morphological classification of neocortical pyramidal cells. *Cerebral Cortex*, 29(4):1719–1735, 2019.
- Kingma, D. P. and Ba, J. Adam: A method for stochastic optimization. In *Proc. of the International Conf. on Learning Representations (ICLR)*, 2015.
- Kipf, T. N. and Welling, M. Semi-supervised classification with graph convolutional networks. In *Proc. of the International Conf. on Learning Representations (ICLR)*, 2017.
- Klicpera, J., Weiß enberger, S., and Günnemann, S. Diffusion improves graph learning. In *Advances in Neural Information Processing Systems (NeurIPS)*, volume 32, 2019.
- Laternus, S. C. and Berens, P. Morphvae: Generating neural morphologies from 3d-walks using a variational autoencoder with spherical latent space. In *Proc. of the International Conf. on Machine learning (ICML)*, volume 139, pp. 6021–6031, 2021.
- Li, Y., Tarlow, D., Brockschmidt, M., and Zemel, R. Gated graph sequence neural networks. *Proc. of the International Conf. on Learning Representations (ICLR)*, 2016.
- Loshchilov, I. and Hutter, F. SGDR: stochastic gradient descent with restarts. *arXiv.org*, 1608.03983, 2016.
- Lu, Y., Carin, L., Coifman, R., Shain, W., and Roysam, B. Quantitative arbor analytics: unsupervised harmonic co-clustering of populations of brain cell arbors based on 1-measure. *Neuroinformatics*, 13(1):47–63, 2015.
- Markram, H., Müller, E., Ramaswamy, S., Reimann, M., Abdellah, M., Aguado, C., Ailamaki, A., Alonso-Nanclares, L., Antille, N., Arsever, S., Guy Antoine, A. K., Berger, T. K., Bilgili, A., Buncic, N., Chalimourda, A., Chindemi, G., Courcol, J.-D., Delalondre, F., Delattre, V., and Schürmann, F. Reconstruction and simulation of neocortical microcircuitry. *Cell*, 163:456–492, 2015.
- Narayanan, A., Chandramohan, M., Venkatesan, R., Chen, L., Liu, Y., and Jaiswal, S. graph2vec: Learning distributed representations of graphs. *arXiv.org*, 1707.05005, 2017.
- Oberlaender, M., de Kock, C. P. J., Bruno, R. M., Ramirez, A., Meyer, H. S., Dercksen, V. J., Helmstaedter, M., and Sakmann, B. Cell Type-Specific Three-Dimensional Structure of Thalamocortical Circuits in a Column of Rat Vibrissal Cortex. *Cerebral Cortex*, 22(10):2375–2391, 2012.
- Oord, A. v. d., Li, Y., and Vinyals, O. Representation learning with contrastive predictive coding. *arXiv.org*, 1807.03748, 2018.
- Paszke, A., Gross, S., Massa, F., Lerer, A., Bradbury, J., Chanan, G., Killeen, T., Lin, Z., Gimelshein, N., Antiga, L., Desmaison, A., Kopf, A., Yang, E., DeVito, Z., Raison, M., Tejani, A., Chilamkurthy, S., Steiner, B., Fang, L., Bai, J., and Chintala, S. Pytorch: An imperative style, high-performance deep learning library. In *Advances in Neural Information Processing Systems (NeurIPS)*, 2019.
- Pedregosa, F., Varoquaux, G., Gramfort, A., Michel, V., Thirion, B., Grisel, O., Blondel, M., Prettenhofer, P., Weiss, R., Dubourg, V., Vanderplas, J., Passos, A., Cournapeau, D., Brucher, M., Perrot, M., and Duchesnay, E. Scikit-learn: Machine learning in Python. *Journal of Machine Learning Research (JMLR)*, 12:2825–2830, 2011.
- Polavaram, S., Gillette, T. A., Parekh, R., and Ascoli, G. A. Statistical analysis and data mining of digital reconstructions of dendritic morphologies. *Frontiers in neuroanatomy*, 8:138, 2014.
- Qiu, J., Chen, Q., Dong, Y., Zhang, J., Yang, H., Ding, M., Wang, K., and Tang, J. Gcc: Graph contrastive coding for graph neural network pre-training. In *Proc. of Conf. on Knowledge Discovery and Data Mining (KDD)*, pp. 1150–1160, 2020.
- Ramaswamy, S., Courcol, J.-D., Abdellah, M., Adaszewski, S. R., Antille, N., Arsever, S., Atenekeng, G., Bilgili, A., Brukau, Y., Chalimourda, A., Chindemi, G., Delalondre, F., Dumusc, R., Eilemann, S., Gevaert, M. E., Gleeson, P., Graham, J. W., Hernando, J. B., Kanari, L., Katkov, Y., Keller, D., King, J. G., Ranjan, R., Reimann, M. W., Rössert, C., Shi, Y., Shillcock, J. C., Telefont, M., Van Geit, W., Villafranca Diaz, J., Walker, R., Wang, Y., Zaninetta, S. M., DeFelipe, J., Hill, S. L., Müller, J., Segev, I., Schürmann, F., Müller, E. B., and Markram, H. The neocortical microcircuit collaboration portal: a resource for rat somatosensory cortex. *Frontiers in Neural Circuits*, 9:44, 2015.

- Ramón y Cajal, S. *Histologie du système nerveux de l'homme et des vertébrés*. 1911.
- Scala, F., Kobak, D., Bernabucci, M., Bernaerts, Y., Cadwell, C., Castro, J., Hartmanis, L., Jiang, X., Lathunus, S., Miranda, E., Mulherkar, S., Tan, Z., Yao, Z., Zeng, H., Sandberg, R., Berens, P., and Tolias, A. Phenotypic variation of transcriptomic cell types in mouse motor cortex. *Nature*, 598:1–7, 2021.
- Scarselli, F., Gori, M., Tsoi, A. C., Hagenbuchner, M., and Monfardini, G. The graph neural network model. *IEEE transactions on neural networks*, 20(1):61–80, 2008.
- Scarselli, F., Gori, M., Tsoi, A. C., Hagenbuchner, M., and Monfardini, G. The graph neural network model. *IEEE Transactions on Neural Networks*, 20(1):61–80, 2009.
- Schubert, P., Dorckenwald, S., Januszewski, M., Jain, V., and Kornfeld, J. Learning cellular morphology with neural networks. *Nature Communications*, 10:2736, 2019.
- Scorcioni, R., Polavaram, S., and Ascoli, G. A. L-measure: a web-accessible tool for the analysis, comparison and search of digital reconstructions of neuronal morphologies. *Nature protocols*, 3(5):866–876, 2008.
- Seshamani, S., Elabbady, L., Schneider-Mizell, C., Mahalingam, G., Dorckenwald, S., Bodor, A., Macrina, T., Bumbarger, D., Buchanan, J., Takeno, M., Yin, W., Brittain, D., Torres, R., Kapner, D., Lee, K., Lu, R., Wu, J., daCosta, N., Reid, R. C., and Collman, F. Automated neuron shape analysis from electron microscopy. *arXiv.org*, 2006.00100, 2020.
- Sun, F.-Y., Hoffmann, J., and Tang, J. Dendritic organization in the neurons of the visual and motor cortices of the cat. *Journal of Anatomy*, 87:387–406, 1953.
- Sun, F.-Y., Hoffmann, J., and Tang, J. Infograph: Unsupervised and semi-supervised graph-level representation learning via mutual information maximization. In *Proc. of the International Conf. on Learning Representations (ICLR)*, 2020.
- Uylings, H. B. and Van Pelt, J. Measures for quantifying dendritic arborizations. *Network: computation in neural systems*, 13(3):397, 2002.
- van der Maaten, L. and Hinton, G. Visualizing data using t-sne. *Journal of Machine Learning Research (JMLR)*, 9 (86):2579–2605, 2008.
- Vaswani, A., Shazeer, N., Parmar, N., Uszkoreit, J., Jones, L., Gomez, A. N., Kaiser, L., and Polosukhin, I. Attention is All you Need. *Advances in Neural Information Processing Systems (NeurIPS)*, 2017.
- Veličković, P., Cucurull, G., Casanova, A., Romero, A., Liò, P., and Bengio, Y. Graph Attention Networks. In *Proc. of the International Conf. on Learning Representations (ICLR)*, 2018.
- Veličković, P., Fedus, W., Hamilton, W. L., Liò, P., Bengio, Y., and Hjelm, R. D. Deep graph infomax. In *Proc. of the International Conf. on Learning Representations (ICLR)*, 2019.
- Wang, Y. A simplified morphological classification scheme for pyramidal cells in six layers of primary somatosensory cortex of juvenile rats. *IBRO Reports*, 5, 2018.
- Xu, M., Wang, H., Ni, B., Guo, H., and Tang, J. Self-supervised graph-level representation learning with local and global structure. In *Proc. of the International Conf. on Machine learning (ICML)*, volume 139, pp. 11548–11558, 2021.
- Zhang, J., Zhang, H., Xia, C., and Sun, L. Graph-bert: Only attention is needed for learning graph representations. *arXiv.org*, 2001.05140, 2020.
- Zhu, Y., Xu, Y., Yu, F., Liu, Q., Wu, S., and Wang, L. Graph contrastive learning with adaptive augmentation. In *Proceedings of the Web Conference 2021*, pp. 2069–2080, 2021.

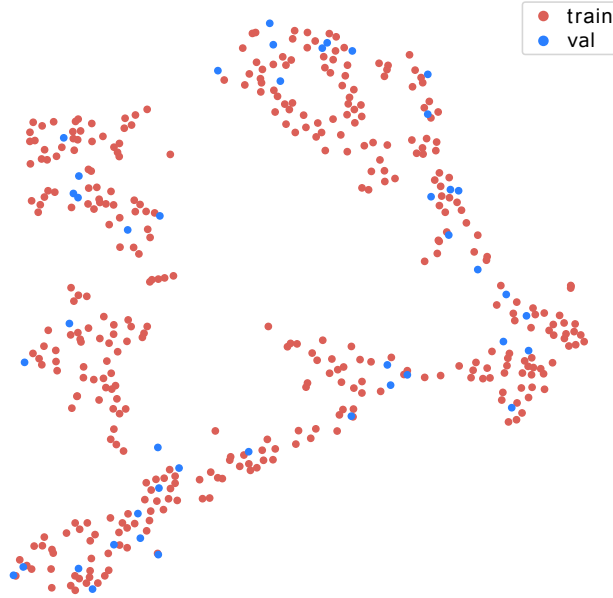


Figure A.1. t-SNE embedding of ABA dataset colored by data from the training and validation set.

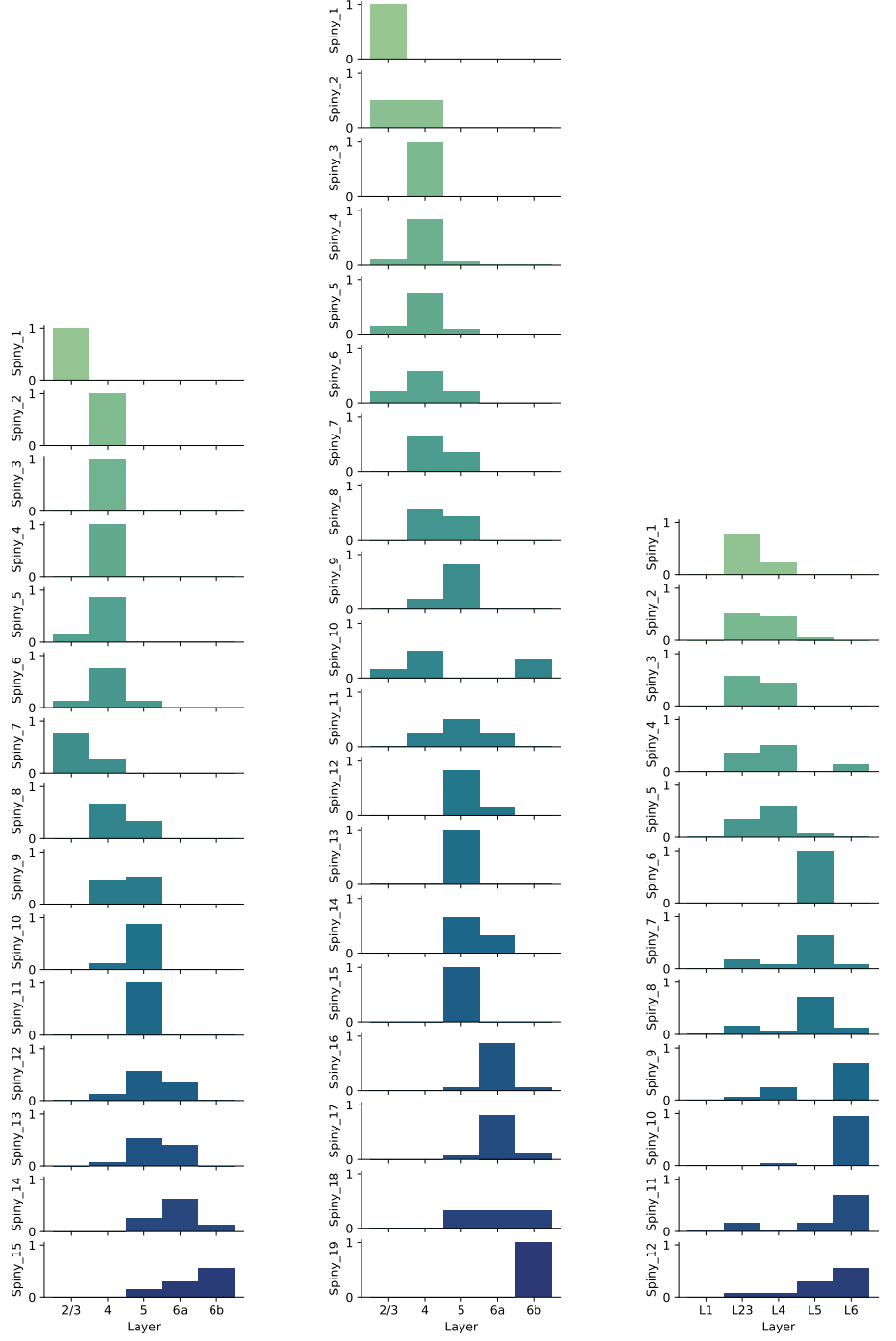
Appendices

A. Additional results

B. Ablation studies

To verify our modeling choices, we perform the following ablation studies: (1) changing the attention to standard transformer attention (Vaswani et al., 2017) and (2) removing the positional encoding. To determine the reliance of our model on different node features, we perform further ablation studies: (1) removing soma depth information by normalizing the y-axis by the soma depth and (2) removing information about neural compartments of nodes. Moreover, we run an ablation study to examine the influence of separate augmentation strategies (Tab. 1).

To evaluate the performance, we treat the Gouwens et al. (2019) labels as if they were ground truth and train a random forest classifier to predict those from the latent representations. Note that this is only a proxy for performance since the labels do not actually correspond to ground truth labels. Nevertheless, we observe a reasonable correlation between the metric and qualitative evaluation of t-SNE embeddings. For scalability to as many ablations as possible, we therefore choose to use this quantitative metric. To minimize the variability over the training of the random forest classifier, we run the training over 100 random seeds and report average performance. For each seed, the classifier is trained using 10-fold cross-validation.



(a) Distribution of cortical layers of origin in our clusters for ABA dataset.

(b) Distribution of cortical layers of origin in each Gouwens et al. (2019) cluster for ABA dataset.

(c) Distribution of cortical layers of origin in our clusters for BBP dataset.

Figure A.2. Distribution of cortical layers of origin.

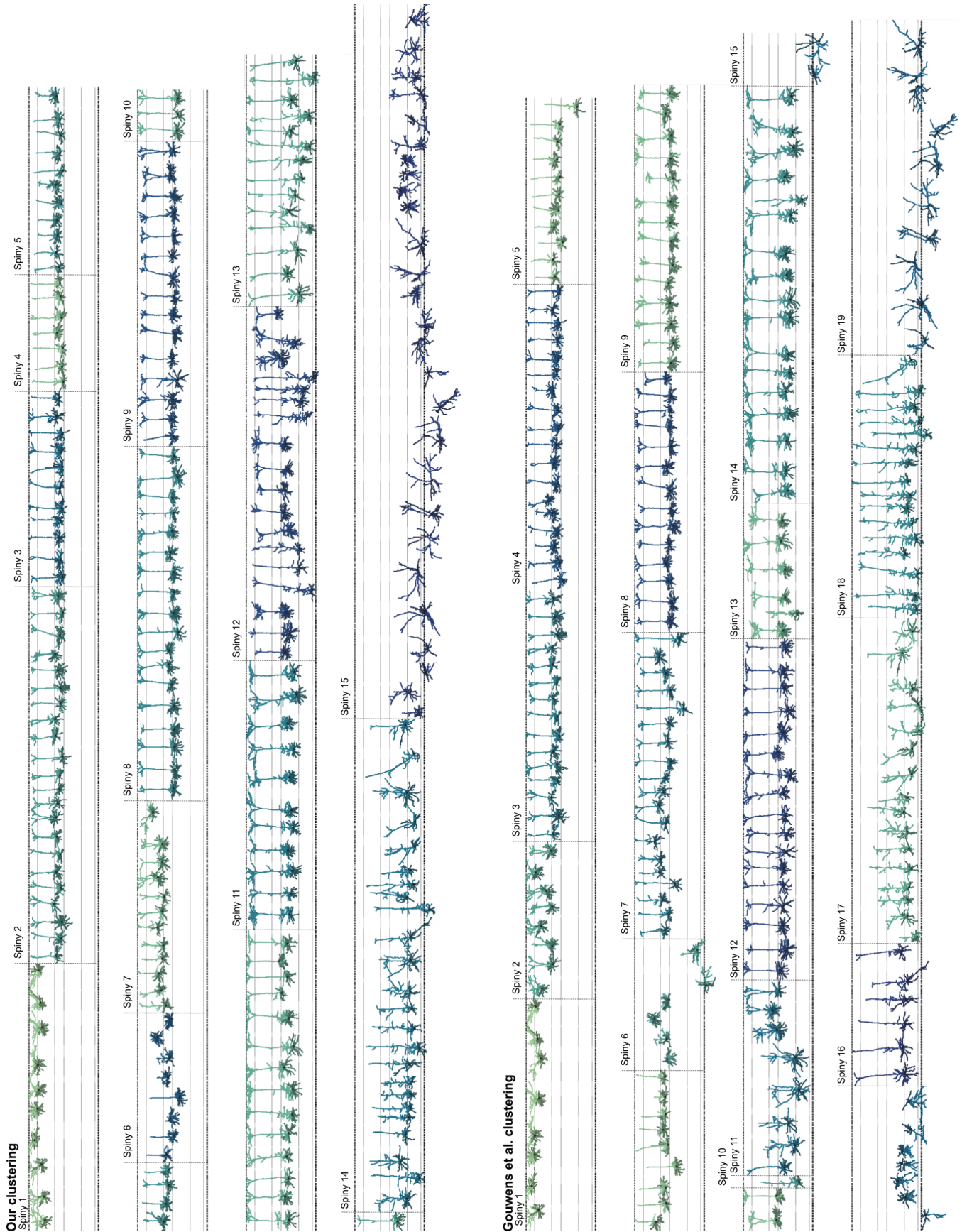


Figure B.3. Clusters of spiny neurons of the ABA dataset as identified by our clustering (rows 1–4) and Gouwens et al. (2019) clustering (rows 5–8). Apical dendrites are colored lighter, while basal dendrites are shown in a darker color. Soma is marked by a black circle.

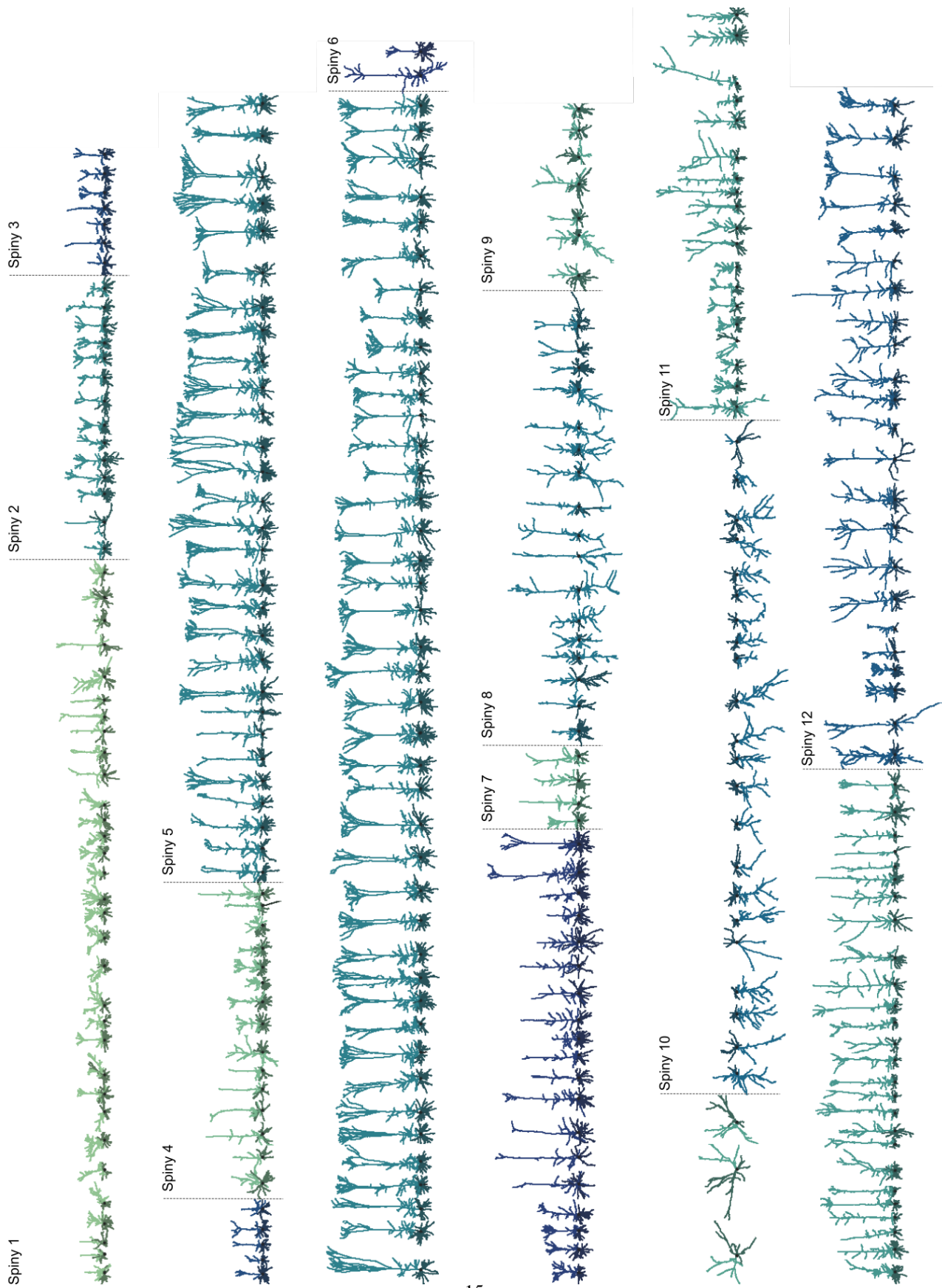


Figure B.4. Clusters of spiny neurons of BBP dataset as identified by GMM based on our learned feature space. Apical dendrites are colored lighter, while basal dendrites are shown in a darker color. Soma is marked by a black circle.